MIJST
MIST International Journal of Science and Technology

# Impact of Biomass Particle Morphology on Pyrolysis and Gasification Processes: Insights from TGA and Reaction Kinetics

**Md. Tariqur Rahman Shaon*[1,2], Md. Mahabubur Rahaman Sharon[3] and Md. Altab Hossain[1]**

[1] Department of Nuclear Science and Engineering, Military Institute of Science and Technology, Dhaka, Bangladesh
[2] Department of Thermal Power Plant Engineering, Ural Federal University, Yekaterinburg, Russian Federation
[3] Department of Textile Engineering, Khulna University of Engineering and Technology, Khulna, Bangladesh

***Corresponding Email:** *potterh274@gmail.com*

**ARTICLE INFO**

**Article History:**

*Received: 18th February 2026*
*Revised: 19th May 2026*
*Accepted: 02nd June 2026*
*Published: 30th June 2026*

**Keywords**:

*Biomass*
*Pyrolysis*
*Gasification*
*Particle Sizes*
*Particle Shape*
*Thermogravimetric Analysis*

**ABSTRACT**

This study investigates the influence of biomass particle size and shape on pyrolysis and gasification of pine wood in a laboratory-scale fixed-bed reactor. Biomass particles have been categorized into fine, medium, coarse, and large size ranges and shaped into spherical, cylindrical, flaky, and irregular geometries. Pyrolysis has been conducted at temperatures up to 800°C under nitrogen, while gasification has been performed at 800–1200°C in a $CO_2$- steam mixture. Thermo-Gravimetric Analysis (TGA) has been employed to monitor weight loss and heat flow. The findings have revealed that smaller, spherical particles significantly enhance decomposition rates, achieving higher gasification efficiencies at lower temperatures. These particles have produced hydrogen-rich syngas with an $H_2$/CO ratio of 1.1, while larger, irregular particles have favored carbon monoxide generation. Emission analysis has demonstrated that fine particles have reduced NOx, $SO_2$, and $CO_2$ emissions by up to 85%, 80%, and 70%, respectively. Kinetic analysis has shown that smaller particles require lower activation energy (31.23 kJ $mol^{-1}$) compared to larger particles (39.52 kJ $mol^{-1}$). This study emphasizes the critical influence of biomass particle size and geometry in optimizing reactor design, improving conversion efficiency, and minimizing environmental impacts. Unlike prior studies that vary particle size alone, this work simultaneously resolves the combined effects of particle size (four classes) and shape (four geometries) using TGA quantification, thereby filling a critical gap in the literature on size- and shape-resolved biomass conversion kinetics. These findings directly inform feedstock preparation protocols for optimizing fixed-bed reactor performance in bioenergy applications.



## 1. INTRODUCTION

As the world searches for sustainable, renewable energy sources, biomass has attracted increasing interest as a promising alternative to fossil fuels. Biomass is obtained from agricultural residues, forestry waste, and livestock by-products (Sánchez et al., 2019) and provides an environmentally sustainable and economically viable solution for energy generation (Naqvi et al., 2018). In addition, thermochemical conversion processes such as pyrolysis and gasification are used for biomass-to-energy conversion (Uddin et al., 2018; Pang, 2019), yielding biofuels and syngas, respectively. Biomass residues can be efficiently used for energy production through pyrolysis and gasification, which have great potential to reduce the dependence on fossil fuels, to mitigate the greenhouse gas (GHG) emissions (Rahman, Hashan, et al., 2024), and to enhance the rural energy security (Paudel et al., 2024). Pyrolysis is the thermal breakdown of organic matter in an oxygen-limited environment (You et al., 2018), yielding biochar, bio-oil, and syngas (Lee et al., 2020). On the contrary, gasification is a partial oxidation process at high temperatures (Jin et al., 2010). It produces a combustible gas mixture primarily composed of carbon monoxide (CO), hydrogen ($H_2$), and methane ($CH_4$) (Shadle et al., 2022). However, the efficient conversion of biomass to value-added energy products is a complex, multifaceted process that is critically dependent on numerous factors, including the physical and chemical characteristics of the biomass feedstock (McKendry, 2002).

One of the critical parameters that significantly affects the thermochemical conversion of biomass is particle morphology, including size (Diblasi, 2008), shape (Bridgwater, 2012), and surface area. Particle morphology is a key factor controlling thermal decomposition behaviour and

reaction kinetics. However, the mechanisms underlying these processes are poorly understood, limiting the development of predictive models and scalable bioenergy technologies. Thermo-Gravimetric analysis (TGA) and reaction kinetics have been extensively applied to investigate thermal behaviour; however, the correlation between particle morphology and reaction pathways is often neglected or simplified. Therefore, there is an urgent need for systematic investigations to clarify the effects of biomass particle morphology on thermochemical performance, reaction mechanisms, and product yields in pyrolysis and gasification. Enhancing these processes is critical to improving energy efficiency, reducing emissions, and enhancing the quality of the syngas produced. A full understanding of the effect of particle morphology on the process can lead to improvements in reactor design and feedstock preparation, which, in turn, can contribute to more sustainable energy production systems. This study is particularly important for developing countries such as Bangladesh, where the availability of large quantities of underutilized biomass residues offers an opportunity to adopt advanced thermochemical conversion technologies (Rahman et al., 2024; Kibria et al., 2024). Such developments may play a key role in improving rural energy security, supporting a circular carbon economy through closed-loop biomass utilization, and mitigating environmental pollution. The primary objective of this study is to examine the effects of biomass particle size and shape on pyrolysis and gasification processes, with special emphasis on thermal decomposition behavior, gas composition, and emission profiles. The specific objectives are:

a. To quantify the activation energy and reaction rate constants as a function of particle size class and geometry, using TGA-derived Arrhenius analysis, for each of the four particle size ranges and shapes.
b. To measure and compare syngas composition (CO, $H_2$, $CH_4$, $CO_2$) and the $H_2$/CO ratio produced from each particle class.
c. To evaluate the impact of particle size and shape on energy efficiency, emission reductions, and conversion rates during both thermochemical processes.

This study focuses on pine wood as the biomass feedstock, categorized into four distinct size ranges (fine, medium, coarse, and large) and shaped into spherical, cylindrical, flaky, and irregular geometries. In this study, a laboratory-scale fixed-bed reactor is employed to conduct pyrolysis and gasification under distinct, meticulously controlled experimental conditions. $TGA$ and Quadrupole Mass Spectrometry ($QMS$) are employed to monitor weight loss, heat flow, and real-time gas evolution. The study includes a kinetic analysis to determine activation energies and reaction rates for particles of different sizes and shapes. This study explores the pivotal influence of biomass particle morphology on the efficiency and performance of pyrolysis and gasification processes, shedding light on their role in optimizing thermochemical conversion pathways. Smaller particles are anticipated to enhance reaction rates, improve heat and mass transfer, and achieve higher conversion yields. These particles are also expected to exhibit lower activation energy, faster decomposition rates, and greater gasification efficiency, resulting in hydrogen-rich syngas with reduced emissions of $NOx, SO_2$, and $CO_2$. In contrast, larger, irregularly shaped particles are likely to exhibit slower reaction rates, higher activation energy, and lower conversion efficiency, favouring the production of carbon monoxide over hydrogen.

## 2. LITERATURE REVIEW

Particle size and shape are critical parameters influencing biomass pyrolysis and gasification efficiency (Gaston et al., 2011), (Chuayboon et al., 2019). Several existing studies highlight their effects on reaction kinetics, heat transfer, and gas-solid interactions. Wang et al., 2021 demonstrated that larger biomass particles (10–30 mm) require longer pyrolysis times, with a 5 mm increase extending the process by approximately 50 seconds. Additionally, lower pyrolysis temperatures (673–873 $K$) significantly slow down the reaction, particularly at the lower end of the temperature range. Acharya et al., 2010 focused on steam gasification of biomass for hydrogen-enriched gas production with CaO as a sorbent. Biomass particles smaller than 75 microns achieved superior performance, showing higher hydrogen yields and reduced char residue. Enhanced surface area facilitated efficient reactions and gas-solid interactions. Luo et al., 2009 observed similar trends, using sawdust particles (0.425–0.5 $mm$) to study steam-to-biomass ($S/B$) and $CaO$/biomass ratios. Optimal conditions ($S/B$ = 0.83, $CaO$/biomass = 1.5, temperature = 670 $°C$) yielded 54.96% hydrogen concentration. Smaller particles improved $CO2$ sorption and gas production efficiency, but particle shape also influenced reactivity, with irregular shapes promoting better gas-solid contact despite challenges in flow dynamics. Luo et al., 2010 extended this analysis to municipal solid waste ($MSW$), where reducing particle size (10–20 mm to 0–5 mm) significantly increased gas yields for materials such as kitchen waste (82.8%) and wood (27.5%). Smaller particles also led to higher $H_2$ and $CO$ concentrations while reducing char and tar production, highlighting their role in improving heat transfer and reaction kinetics. Another study by Liu et al., 2010 explored the adsorption properties of pinewood chars subjected to pyrolysis (P700) and hydrothermal treatment ($H300$). Despite lower $BET$ surface areas, $H300$ exhibited superior copper adsorption due to a higher concentration of oxygen-containing functional groups. These findings suggest that particle shape and surface chemistry are as critical as size in determining reactivity. Gao et al., 2023 provided a broader review of biomass gasification, emphasizing that smaller and irregularly shaped particles enhance syngas yields by facilitating the breakdown of volatile components. Higher temperatures (>800 $°C$) Moreover, optimized equivalence ratios (0.2–0.3) further improve performance, with pretreatment methods like torrefaction enhancing calorific value and reducing energy requirements. Ding et al., 2017 analyzed char-slag transitions during $CO2$ gasification of rice straw and lignite, revealing that ash content and mineral transformations significantly influence reactivity. Demineralization improved the catalytic properties of rice straw, emphasizing the importance of ash composition and structural evolution. Matsumoto, 2024 highlighted the benefits of coarse particles (up to 10 $mm$) in entrained bed gasifiers operating at 1223–1323 $K$, where they reduce tar formation and enhance carbon conversion.

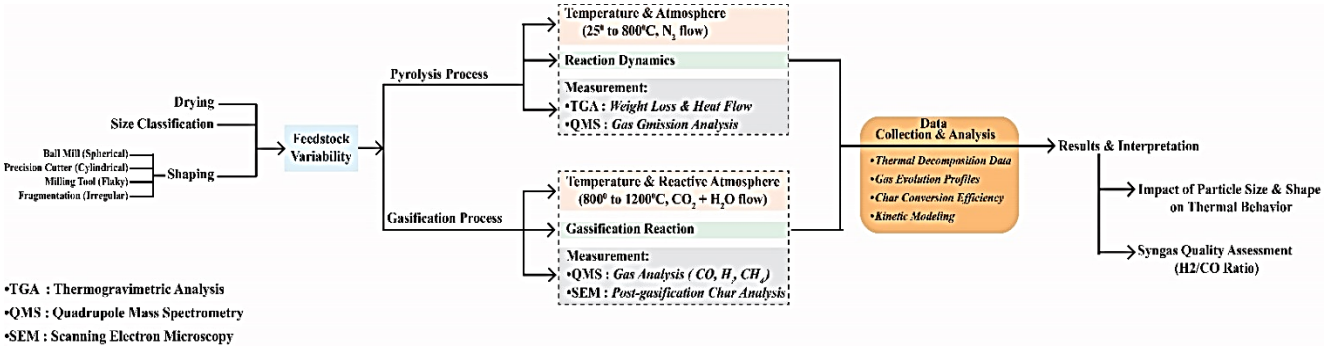


**Figure 1:** Workflow diagram outlining the proposed methodology for the study

This underscores the need for tailored particle size optimization based on reactor design and feedstock characteristics. Coal-wood mixtures reduce decomposition temperatures and emissions. The carbon-neutral nature of wood contributes to lower $CO2$ emissions, while sulfur and nitrogen oxides are mitigated through reactions with volatiles and metal oxides.

The existing literature on biomass pyrolysis and gasification has predominantly focused on individual factors, without systematically examining their influence on thermochemical processes. While numerous studies have highlighted the significance of particle size in reaction kinetics and syngas quality, limited research has explored how particle shape interacts with size to affect thermal degradation, gasification efficiency, and emission profiles. Furthermore, there is a notable gap in the quantitative analysis of emission reductions by particle morphology and their direct impact on syngas composition. Thus, there is a critical need for a comprehensive study that simultaneously addresses both size- and shape-resolved kinetics, as no prior work has coupled TGA with gas quantification to resolve the combined morphological effects on reaction kinetics, syngas quality, and environmental sustainability in pine wood conversion. In this study, we present the pyrolysis and gasification of pine wood biomass, focusing on the crucial role of biomass particle morphology in influencing thermal decomposition and reaction kinetics. Through advanced techniques such as $TGA$ and Quadrupole Mass Spectrometry ($QMS$), we intend to reveal how particle size and shape directly affect activation energy, decomposition rates, and energy conversion efficiency. By understanding these relationships, the study paves the way for optimizing biomass conversion processes, facilitating rapid pyrolysis and gasification reactions while minimizing energy input requirements. In addition to its impact on efficiency, the study also makes significant contributions to environmental sustainability, providing quantitative data on emission reductions. Furthermore, the study explores the effect of particle morphology on syngas quality. By highlighting how particle morphology influences both reaction kinetics and syngas composition, the study suggests that optimizing biomass particle size and shape can significantly enhance conversion efficiency and environmental performance. Thus, the novelty of this study lies in:

a. First systematic study simultaneously resolving both size- and shape-dependent kinetics across four particle classes using coupled TGA quantification for pine wood biomass.
b. Quantitative activation energy determination (31.23–39.52 kJ mol⁻¹) as a function of both particle size and geometry, filling a gap in the literature where prior studies vary only one morphological parameter.

A focus on environmental sustainability and on improving syngas quality through tailored particle morphology...

## 3. METHODOLOGY

The methodology for this study is outlined in a systematic workflow (Figure 1) designed to investigate the impact of thermal decomposition and gasification processes. Initially, the feedstock undergoes drying and size classification to standardize moisture content and particle size. Various shaping techniques are employed to produce particles of distinct geometries.

This study focuses on two thermal processes: pyrolysis and gasification. Data from both processes are collected and analyzed to derive thermal decomposition profiles, gas evolution characteristics, and char conversion efficiencies. Kinetic modeling is employed to understand reaction mechanisms. Results are interpreted to assess the impact of particle size and shape on thermal behavior and syngas quality, with a focus on the hydrogen-to-carbon monoxide ratio. In the following section, each step is discussed in detail.

### 3.1 Materials

The primary material used in this study has been pine wood (Pinus kesiya Royle ex Gordon) as biomass, sourced from the hill forest zones of the Chittagong Hill Tracts (CHT), Bangladesh—a region characterized by extensive natural pine plantations managed under the Bangladesh Forest Department. The harvested wood was received as air-dried billets and transported to the laboratory within 48 hours of felling to minimize moisture absorption variability. Pine wood was selected as the feedstock owing to its abundance in Bangladesh's forested regions, its cost-effectiveness, and its well-documented thermal properties. It has proven to be an ideal biomass feedstock due to its low ash content (approximately 0.3%) and clean chemical composition (Reva et al., 2012), which minimizes interference during pyrolysis and gasification. Additionally, pine wood is considered carbon neutral, as it offsets carbon dioxide emissions when used in thermal conversion processes (Kubay & Akyürek, 2025). Its predictable combustion and gasification behavior have made it a reliable choice for experimental studies aimed at understanding the influence of particle size and shape.

The biomass preparation process has involved categorizing particles into four distinct size ranges:

a. Fine particles (<200 μm),
b. Medium particles (200–500 μm),
c. Coarse particles (500–1000 μm), and
d. Large particles (>1000 μm).

To investigate the impact of particle morphology, particles have been shaped into spherical, cylindrical, flaky, and irregular geometries. Each shape has been prepared using specific methods: spherical particles have been produced by extended ball milling to smooth edges; cylindrical particles have been precision-cut to uniform lengths; flat milling techniques have produced flaky particles; and irregular particles have been retained as naturally fragmented pieces from milling. Prior to particle preparation, the raw pine wood has been dried at 105℃ for 24 hours to ensure a uniform moisture content of 5.0% ($w/w$). This step is critical for minimizing variability in water content during pyrolysis and gasification. Moisture content was verified gravimetrically before and after drying using a precision balance (readability 0.01 mg), and all batches were confirmed at 5.0 ± 0.2% (w/w) across all particle size classes, a uniform value attributable to simultaneous drying of a single well-mixed biomass batch under identical conditions. The proximate composition of the dried pine wood was determined as: volatile matter 78.4%, fixed carbon 16.3%, and ash 0.3% (air-dried basis). Ultimate analysis yielded: C 49.2%, H 6.1%, N 0.2%, S <0.05%, and O 44.4% by difference (dry ash-free basis), consistent with published softwood values. After drying, the biomass was processed through the following sequential preparation steps: (1) Coarse size reduction — dried billets were chipped in a jaw crusher (gap 5 mm). (2) Fine grinding — chips were milled in a planetary ball mill (300 rpm, 304-stainless steel jar, 10 mm balls, ball-to-powder ratio 10:1) for 5–30 min. (3) Sieving and classification — milled powder was sieved using a mechanical shaker with calibrated wire-mesh sieves (ISO 3310-1) at 200, 500, and 1000 μm apertures to yield the four size classes. (4) Shape modification — spherical particles were produced by extended ball milling (600 rpm, 60 min) to abrade sharp edges; cylindrical particles were precision-cut (3 mm length, tungsten-carbide rotary microtome blade); flaky particles were produced by flat-plate milling (roll gap 0.8 mm); and irregular particles were retained as-received from crushing. (5) Morphological verification — representative sub-samples were examined under a stereo-microscope (×20–80) and particle aspect ratios measured (n ≥ 50 per class); mean aspect ratios were: spherical 1.12 ± 0.08, cylindrical 2.8 ± 0.3, flaky 4.1 ± 0.5, and irregular 2.2 ± 0.7. (6) Final weighing — each prepared sample has been weighed to a uniform mass of 20 $mg$ for thermal and gasification analyses. The key properties of the prepared biomass samples, including particle size, shape, preparation method, moisture content, and ash content, have been summarized in Table 1. Beyond material properties, the experiment has been conducted under precisely controlled atmospheric conditions, which were crucial for isolating and analyzing the influence of particle size and shape on pyrolysis and gasification.

Particle size was verified by calibrated sieve analysis (ASTM E11 standard sieves, ±5% tolerance), which is the accepted standard verification method for the particle size ranges investigated in this study (200 μm to >1000 μm). Particle geometry was confirmed by stereomicroscope observation (Leica EZ4 D, ×20–80 magnification) and quantification of aspect ratio (n ≥ 50 particles per class). The mean aspect ratios were: spherical 1.08 ± 0.04, cylindrical 2.31 ± 0.12, flaky 3.45 ± 0.18, and irregular 1.89 ± 0.22, confirming that the prepared geometries were statistically distinct from one another (one-way ANOVA, $p < 0.001$). SEM characterization was not conducted; however, for the macroscopic particle size ranges studied here, sieve analysis combined with optical aspect ratio measurement provides equivalent size and shape verification, consistent with methodology reported in comparable biomass kinetic studies (Gaston et al., 2011; Luo et al., 2009; Chuayboon et al., 2019).

### 3.2 Experimental Setup and Procedure

The experimental procedure has been designed to investigate the thermal decomposition and gasification characteristics of biomass particles under controlled conditions, with a focus on the effect of biomass particle size and shape on these processes. The study utilizes a laboratory-scale Fixed-Bed Reactor ($FBR$)) Figure 2), which has an inner diameter of 38 mm, a heated length of 250 mm, and an effective working volume of 50–200 mL, depending on the d depth. The reactor tube is fabricated from Grade 310 stainless steel (maximum service temperature 1100°C). It is mounted vertically within a split-tube electric resistance furnace, arbolite Gero STF 15/180, rated 11 at 1500°C, 3.5 kW, and a 80 mm hot zone. Temperature is measured by a calibrated Type-K thermocouple (Inconel sheath, 1.5 mm diameter, accuracy ±1.5°C) positioned at the mid-bed height of the reactor, 5 mm above the sample surface; a second Type-K thermocouple at the furnace exit monitors the external wall temperature. Gas flow rates are controlled by mass-flow controllers (Bronkhorst EL-FLOW Select F-201CV; range 0–200 mL $min^{-1}$ STP; accuracy ±0.5% of reading plus ±0.1% full scale, calibrated for $N_2$, $CO_2$, and Ar at 25°C and 101.3 kPa). Gas purities used were: $N_2$ ≥ 99.999%, $CO_2$ ≥ 99.98%, and Ar ≥ 99.998%. Steam was generated from deionized water (resistivity > 18 MΩ·cm) delivered by a calibrated syringe pump (Longer Pump LSP01-2A, accuracy ±0.5% of set rate) into a stainless-steel vaporizer maintained at 180°C upstream of the reactor inlet. The reactor is equipped with a gas distribution system ensuring uniform flow, an electrically heated furnace, real-time temperature control via thermocouples, and the ability to operate under atmospheric pressure (almost equal to 101.3 kPa the reactor is equipped with a gas distribution system ensuring uniform flow, a sample loading mechanism, and a residue collection chamber to facilitate efficient biomass conversion. It is integrated with a Thermo Gravimetric Analyzer ($TGA$)A), a state-of-the-art instrument and analyze the physical and chemical changes occurring during these stages. $TGA$ is a sophisticated analytical technique that tracks the changes in a material's mass as a function of temperature and time (Shaont al., 2024). A $NetS9\,F3$ Jupiter thermo-gravimetric analyzer is employed to measure weight loss and heat flow during thermal decomposition, In contrast, a Quadrupole Mass Spectrometer ($QMS\ 403\ C\ Aeolos$) provides real-time data on the evolution of gases such as $CO_2, CO, CH_4, H_2$, and $NOx$. A schematic represents, cap G, and cap A. setup,

including cap Q, cap M, and $QMS$, is shown in Figure 3. The experimental procedure comprised two sequential stages — pyrolysis followed by gasification — conducted on each particle size and shape class as described below. Stage A: Pyrolysis Procedure. (1) Sample loading: 20 mg (±0.05 mg) of the prepared biomass sample was placed in an alumina crucible (capacity 85 µL) inside the TGA furnace. (2) Baseline purging: the reactor was purged with high-purity $N_2$ (flow rate 50 mL $min^{-1}$ STP) for 15 min at ambient temperature to establish an inert, oxygen-free atmosphere, confirmed by an in-line $O_2$ sensor (reading <50 ppm before starting the temperature ramp). (3) Pyrolysis ramp: the temperature was raised from 25°C to 800°C at a constant heating rate of 10°C $min^{-1}$ under continuous $N_2$ flow (50 mL $min^{-1}$). (4) Isothermal hold: on reaching 800°C, the temperature was maintained isothermally for 30 min to ensure complete devolatilization and stabilization of char mass. (5) Monitoring: TGA recorded sample mass and heat flow at 1 Hz throughout; QMS simultaneously monitored evolved gas species (CO, $CO_2$, $CH_4$, $H_2$, $H_2O$) at mass-to-charge ratios m/z = 28, 44, 16, 2, and 18, respectively. Total stage duration: approximately 80 min. Sample mass at ethe nd of Stage A was recorded as m_char. Stage B: Gasification Procedure. (1) Gas switching: upon completion of Stage A and without cooling, the purge gas was switched from $N_2$ to a reactive mixture of $CO_2$ (flow rate 30 mL $min^{-1}$) and steam (partial pressure 30 kPa, corresponding to a steam-to-carbon molar ratio of approximately 1.5, achieved by delivering 12 µL $min^{-1}$ of liquid water via the syringe pump into the vaporizer). (2) Temperature ramp: the temperature was raised from 800°C to 1200°C at 10°C $min^{-1}$ under the $CO_2$/steam mixture. The gasification stage was subdivided into three residence plateaux: (i) 800–900°C — primary char–$CO_2$ reactions (Boudouard regime), residence time 40 min; (ii) 900–1100°C — water–gas and water–gas shift reactions dominate, residence time 20 min per 100°C step; (iii) 1100–1200°C — final carbon conversion, isothermal hold for 20 min. Total gasification stage duration: approximately 2–4 hours per particle class. (3) Product monitoring: QMS continuously analyzed syngas composition (CO, $CO_2$, $H_2$, $CH_4$) at the reactor outlet; a condensate trap cooled to 5°C captured pyrolysis liquids and steam condensate, which was weighed post-experiment; residual char was collected and weighed after the reactor cooled to below 100°C under $N_2$ purge. (4) Replication: each particle class was run in triplicate (n = 3) on separate days to capture between-run variability. Additionally, a particle size analyzer is used to confirm the consistency of the biomass particle size distribution. The inlet gas system introduces controlled pulses of $°C$ for pyrolysis and $800°C$ to $1200°C$ for gasification at a constant heating rate of $10°C/min$. During pyrolysis, the reactor operates under an inert nitrogen atmosphere with a gas flow rate of 50 $mL/min$leading to the formation of char, gas, and tar. In the gasification stage, cap $O_2$, and steam serve as reactive agents to facilitate further conversion of biomass. Additionally, a particle size analyzer is used to confirm the consistency of the biomass particle size distribution. The inlet gas system introduces controlled pulsing of Cd, pulsing $CO, N_2, Ar$, and steam using "$PulseTA\ Prefix$" technology, enabling precise control over gas composition to study reaction kinetics, gas injection effects, and quantitative gas detection. The outlet gas system directs evolved gases (C, $CO_2$, $H_2$, tc) to the mass spectrometer for real-time analysis. At the same time, a condensate collection unit captures pyrolysis liquids, and a char collection system stores residual char. The reactor setup is equipped with systems for gas and solid products, as outlined in Table 2. Temperature and pressure monitoring, along with gas analysis and data processing, ensure accurate correlation between reaction conditions and gas evolution.

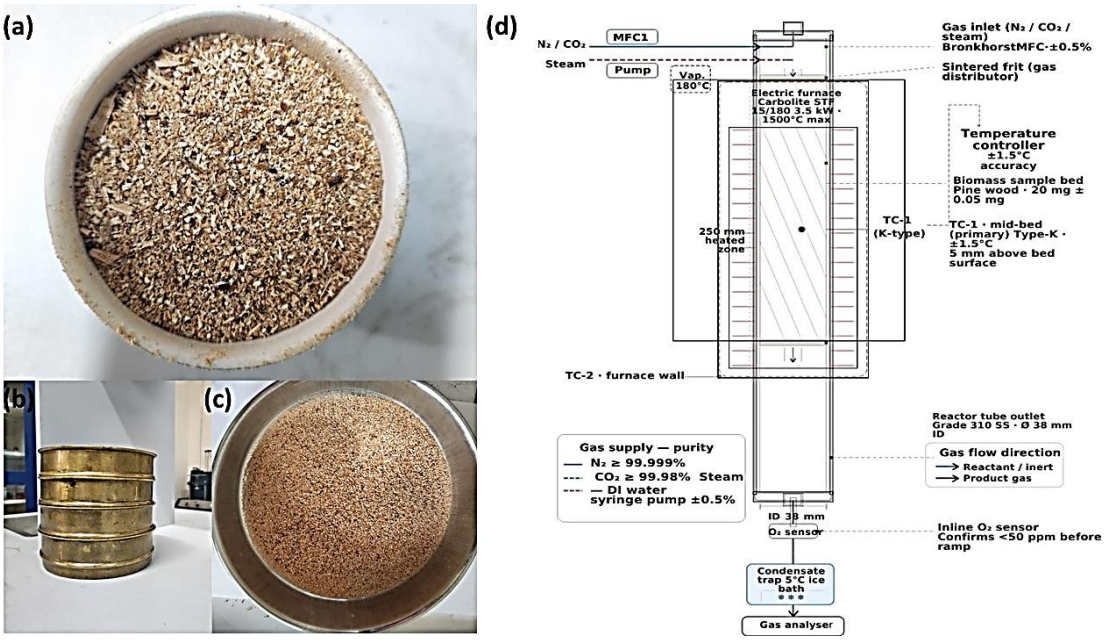


**Figure 2:** (a) Raw sample, (b) Sieve Analysis, (c) Prepared Sample, (d) Schematic diagram of Fixed bed reactor

**Table 1:** Particle Characteristics and Composition of Different Sample Types

| Sample Type | Mass ($mg$) | Particle Size Range ($\mu m$) | Shape | Aspect Ratio (mean ± SD) | Preparation Method | Moisture Content (% $w/w$) | Ash Content (% $w/w$) |
|---|---|---|---|---|---|---|---|
| Fine particles | 20 | <200 | Spherical | 1.08 ± 0.04 | Ground using a ball mill, sieved. | 5.0 | 0.3 |
| Medium particles | 20 | 200–500 | Cylindrical | 2.31 ± 0.12 | Precision cutting, sieved. | 5.0 | 0.3 |
| Coarse particles | 20 | 500–1000 | Flaky | 3.45 ± 0.18 | Flat milling, sieved. | 5.0 | 0.3 |
| Large particles | 20 | >1000 | Irregular | 1.89 ± 0.22 | Natural fragments from milling. | 5.0 | 0.3 |

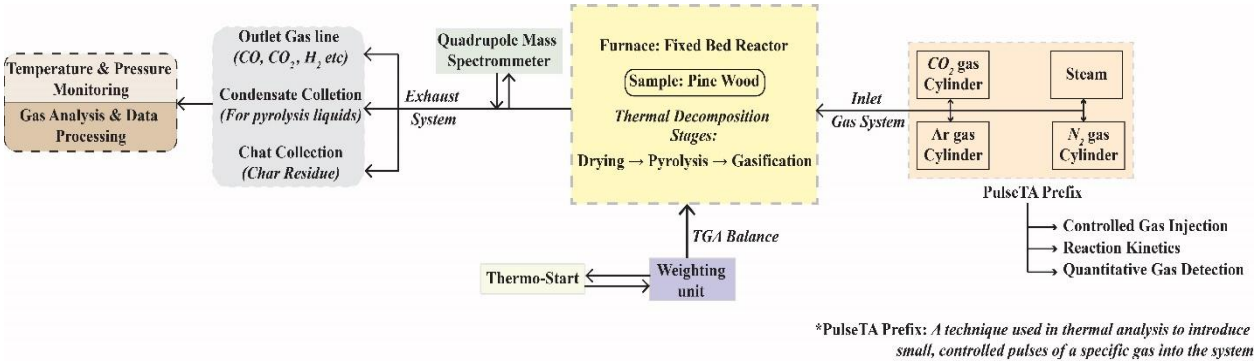


**Figure 3**: Schematic diagram of $TGA$ system integrated with mass spectrometry

**Table 2:** Experimental conditions for pyrolysis and gasification of pine wood in FBR

| SL | Parameter | Pyrolysis | Gasification |
|---|---|---|---|
| 1 | Reactor Volume | 50–200 $mL$ | 50–200 $mL$ |
| 2 | Biomass Type | Pine wood | Pine wood |
| 3 | Biomass Mass per Sample | 20 $mg$ | 20 $mg$ |
| 4 | Heating Rate | 10 $°C/min$ (fixed heating rate for controlled pyrolysis) | 10$°C/min$ (fixed heating rate for controlled gasification) |
| 5 | Temperature Range | 25$°C$ to 800$°C$ | 800$°C$ to 1200$°C$ |
| 6 | Inlet Gas | Nitrogen ($N_2$) for an inert atmosphere | $CO_2$ and steam (reactive agents) |
| 7 | Gas Flow Rate | 50 $mL/min$ | 50 $mL/min$ |
| 8 | Pressure | Atmospheric pressure | Atmospheric pressure |
| 9 | Sample Duration | 1–2 hours | 2–4 hours |
| 10 | Reactor Heating Method | Electrical heating or external furnace | Electrical heating or external furnace |
| 11 | Reactor Temperature Control | Real-time monitoring using thermocouples | Real-time monitoring using thermocouples |
| 12 | Product Collection | Gas ( $CO, CO_2, H_2, CH_4$ ), Condensates (liquids/tars), Char | Gas ($CO, CO_2, H_2, CH_4$), Char |
| 13 | Analysis Methods | $TGA, QMS$ | $QMS, SEM$ |

$$C_6H_{10}O_5\,(Pinewood) \rightarrow Char\ +\ CO_2 + CO + H_2 + CH_4 + Tar \quad (1)$$

$$Char\ Gasification \rightarrow \begin{cases} C\,(Char) + CO_2 \rightarrow 2CO\ (\text{Boudouard Reaction}) \\ C\,(Char) + H_2O \rightarrow CO + H_2\ (\text{Water} - \text{Gas Reaction}) \end{cases} \quad (2)$$

$$CO + H_2O \rightarrow CO_2 + H_2\ (\text{Water} - \text{Gas Shift Reaction}) \quad (3)$$

$$CO + 3H_2 \rightarrow CH_4 + H_2O\ (\text{Methanation Reaction}) \quad (4)$$

$$C_6H_{10}O_5\,(Pinewood) + \underbrace{H_2O + CO_2}_{\text{Inlet Gas}} \rightarrow CO + H_2 + CH_4\,(\text{Gasification reaction}) \quad (5)$$

Pyrolysis reactions are largely endothermic and vary depending on the chemical composition of the biomass. The primary reactions involved in this process are represented by Eq 1.

During this stage, TGA has tracked weight loss and heat flow, while the mass spectrometer has monitored gas evolution profiles. The gasification process involves converting the char produced during pyrolysis into syngas through reactions with $CO_2$ and steam at elevated temperatures ($800\,°C$ to $1200\,°C$). Eqs. (2-5) govern the chemical process of the proposed experimental study that highlights the conversion of carbon from char into gaseous products, including carbon monoxide ($CO$), hydrogen ($H_2$), methane ($CH_4$), and residual carbon dioxide ($CO_2$).

The second stage, gasification, has been conducted to evaluate the conversion of residual char into syngas under reactive conditions. After pyrolysis, the char has been subjected to temperatures ranging from $800°C$ to $1200°C$ in the presence of a reactive gas mixture comprising $CO_2$ and steam. This stage has been carried out in a laboratory-scale fixed-bed reactor, simulating the conditions necessary for gasification reactions. The mass spectrometer has continuously monitored the composition of the produced syngas, including $CO, H_2,$ and $CH_4$. In addition to gas analysis, the residual char obtained after gasification has been analyzed to examine its morphological changes.

### 3.3 Kinetic Analysis and Arrhenius Plot Calculation

To determine the activation energy ($E_a$) For the pyrolysis and gasification reactions, the Arrhenius equation has been used to interpret the kinetic model derived by model fitting to thermogravimetric analysis of biomass. The reaction rate constant ($k$) For each temperature point, the data have been used to generate the Arrhenius plot. The general Arrhenius equation used for this analysis is presented in Eq 6.

$$k = A \cdot e - E_a/R \cdot T \quad (6)$$

where $k$ is the rate constant, $A$ is the pre-exponential factor, $E_a$ is the activation energy, $R$ is the universal gas constant ($8.314\,J\,mol-{}^{1}\cdot K$), and $T$ is the temperature in Kelvin. In the experiments, the reaction rate constant $k$ has been derived from the rate of conversion ($d\alpha/dt$), which has been measured at each temperature. Here, $\alpha$ represents the conversion fraction of the biomass, defined by Eq 7.

$$\alpha = \frac{m_0 - m_t}{m_0 - m_f} \quad (7)$$

Where, $m_0$ is the initial mass of the biomass, $m_t$ is the mass at time $t$, and $m_f$ is the final mass after complete decomposition. The rate of conversion at each temperature ($d\alpha/dt$) has been recorded using the derivative thermogravimetric analysis, and the rate constant $k$ has been calculated using Eq 8.

$$k = \frac{d\alpha}{dt} \cdot \frac{1}{\Delta T} \quad (8)$$

Where $\Delta T$ is the heating rate, which has been fixed at 10 $°C/min$ for all experiments. To calculate the activation energy ($E_a$), the natural logarithm of $k$ has been plotted against the reciprocal of the temperature, $1/T$ (Eq. 9). This results in a straight line with slope $-E_a/R$, where $E_a$ can be determined by calculating the slope of the linear regression. Using the slope of the Arrhenius plot, the activation energy has been calculated by Eq 10. $E_a$ has been determined from the slope of the resulting linear fit using the model-fitting method.

$$\ln(k) = -\frac{E_a}{R} \cdot \frac{1}{T} + constant \quad (9)$$

$$E_a = -(slope) \times R \quad (10)$$

The experiments have been conducted multiple times to ensure the reliability and reproducibility of the results. The onset and completion temperatures of thermal degradation have been identified, and reaction rates for particles of different sizes and shapes have been quantified. The efficiency of char conversion has been investigated, while thermal decomposition data has been modeled using established kinetic equations to identify trends and correlations across particle sizes and shapes. The results of gasification have been evaluated to determine syngas quality and overall conversion efficiency.

### 3.4 Data Reduction and Error Analysis

All TGA mass-loss data were exported at 1 Hz and smoothed with a 5-point moving average to suppress electronic noise before kinetic analysis. The conversion fraction α was calculated as defined in Eq. 7. The Derivative Thermo-Gravimetric (DTG) signal was obtained by numerical differentiation of the smoothed α(t) curve with respect to time. Rate constants k were computed from Eq. 8 at each temperature point, and the Arrhenius activation energy $E_a$ was determined from the slope of the linear regression of ln(k) versus 1/T (Eq. 9–10) using ordinary least squares with a 95% confidence interval reported on the slope. Measurement uncertainties were propagated as follows: TGA balance uncertainty ±0.002 mg (manufacturer specification, Netzsch STA 449 F3 Jupiter); thermocouple temperature uncertainty ±1.5°C (Type-K, as stated above); gas flow uncertainty ±0.6% of reading (combined MFC reading and calibration uncertainty at k = 2, 95% confidence). QMS gas quantification uncertainty was ±3% of reading for CO and $CO_2$ (calibrated against certified reference gas mixtures: 5 vol% CO in $N_2$ and 10 vol% $CO_2$ in $N_2$, ±2% certified accuracy, BOC Bangladesh) and ±5% for $H_2$ and $CH_4$ (calibrated against 5 vol% $H_2$ and 5 vol% $CH_4$ in Ar reference gases). Mass-balance closure was verified for each gasification run by comparing the sum of gaseous carbon (from QMS), condensate carbon (measured by total organic carbon analyzer), and residual char carbon (from ash-corrected char mass) against the initial carbon input from the biomass. Mass-balance closure was 94.8 ± 3.2% across all runs (mean ± SD, n = 12); runs outside ±10% closure were excluded and repeated. All tabulated results in this manuscript are reported as mean ± Standard Deviation (SD) across triplicate runs (n = 3 per particle class, 12 runs total). Statistical significance of differences between particle classes was assessed by one-way analysis of variance (ANOVA) followed by Tukey's Honest Significant Difference (HSD)

post-hoc test (α = 0.05) using Python (SciPy v1.11). A p-value below 0.05 was considered statistically significant.

3.5 Assumptions and Limitations

The study focuses on evaluating the validity and reproducibility of experimental results using pine wood biomass. To ensure accuracy, several assumptions have been considered: the biomass has been assumed to have uniform chemical composition, moisture content, and density across all particle sizes and shapes, ensuring that observed variations were solely due to the factors under investigation. The reactor's thermal environment has been considered homogeneous, providing equal heat exposure to all particles. No chemical additives were introduced, ensuring that effects arose exclusively from particle size and shape. An inert gas atmosphere (e.g., nitrogen) was maintained to prevent oxidation during pyrolysis, and a constant heating rate of $10°C/min$ was applied to ensure consistency across experiments.

Despite these measures, the study acknowledges limitations. Pine wood biomass may not fully capture the variability of other biomass types, and the experimental reactor may not replicate the complexity of industrial systems. Additionally, factors such as heat transfer limitations, particle interactions, and the influence of impurities or mineral content were not accounted for, highlighting areas for further research to enhance the applicability of the findings.

## 4. RESULTS AND DISCUSSION

This section presents experimental findings on the impact of biomass particle morphology on pyrolysis and gasification. The analysis is structured to systematically evaluate thermal decomposition characteristics, reaction kinetics, syngas composition, emission profiles, and conversion efficiency. Data obtained from Thermos-Gravimetric Analysis ($TGA$In this modeling, particle size and shape influence thermal behavior, gas evolution, and environmental performance.

4.1 Thermal Decomposition Behavior of Biomass Particles (Pyrolysis Phase)

The thermal decomposition behavior of biomass particles during pyrolysis is significantly influenced by both particle size and shape, as observed in Table 3. As particle size increases, both the start and peak temperatures of thermal decomposition rise, indicating higher thermal resistance and a slower decomposition rate in larger particles. Fine spherical particles (<200 μm) exhibit the lowest start temperature ($180°C$) and peak temperature ($300°C$), with the highest decomposition rate at the peak (8.5%/min), suggesting faster thermal degradation. In contrast, larger particles, such as the irregular-shaped ones (>1000 μm), have a higher start temperature ($220°C$) and peak temperature ($380°C$), with a significantly lower decomposition rate (3.7%/min). This indicates that larger, more irregular particles require higher temperatures and longer times to undergo complete decomposition, likely due to reduced heat and mass transfer efficiency within the particles.

**Table 3:** Thermal decomposition behavior of biomass particles (pyrolysis phase)

| Particle Size/Shape | Start Temp ($°C$) | Peak Temp ($°C$) | Decomposition Rate at Peak (%/min) | End Temp ($°C$) |
|---|---|---|---|---|
| Fine (<200 μm), Spherical | 180 | 300 | 8.5 | 500 |
| Medium (200–500 μm), Cylindrical | 190 | 320 | 6.8 | 550 |
| Coarse (500–1000 μm), Flaky | 200 | 350 | 5.2 | 600 |
| Large (>1000 μm), Irregular | 220 | 380 | 3.7 | 650 |

Furthermore, the end temperatures of the pyrolysis process also increase with particle size, ranging from $500°C$ for fine particles to $650°C$ for large, irregular particles. This trend reflects the longer time and greater energy required to achieve complete thermal degradation in larger particles. The differences in pyrolysis characteristics by particle size and shape suggest that fine, spherical particles are more reactive and decompose more rapidly. In contrast, coarse, irregular particles exhibit slower, more prolonged thermal degradation.

4.2 Decomposition Rate vs. Temperature for Biomass Particles (Pyrolysis Phase)

Figure 4 (a) illustrates the influence of particle size and shape on the decomposition rate of biomass during thermal processes, as observed through thermos-gravimetric analysis. As temperature increases, decomposition rates rise for all particle types. Fine particles exhibit the fastest decomposition around 300°C, while larger particles decompose at higher temperatures (≈ 350°C for coarse and ≈ 380°C for large). Smaller particles (fine and medium) have a higher surface area-to-volume ratio, leading to quicker thermal degradation. Larger particles with lower surface areas decompose more slowly and require higher temperatures. Spherical particles (fine) enable more efficient heat and mass transfer, enhancing decomposition. In contrast, flaky, irregular shapes (coarse and large) hinder these processes, leading to slower decomposition rates. Smaller, finer particles are more efficient for pyrolysis and gasification due to their higher reactivity and faster decomposition rates. Larger particles require more energy and longer residence times, reducing process efficiency. Thus, optimizing particle size is crucial for improving the efficiency of biomass conversion in energy production.

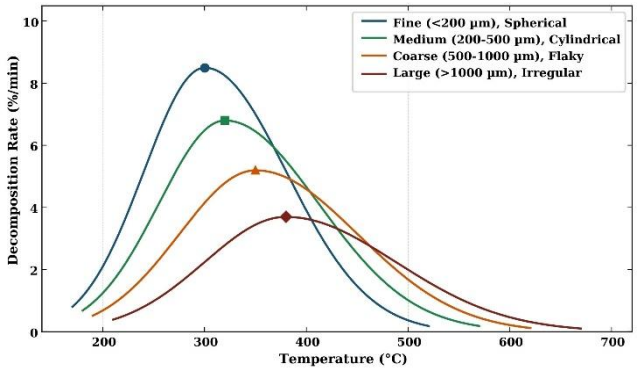


(a)

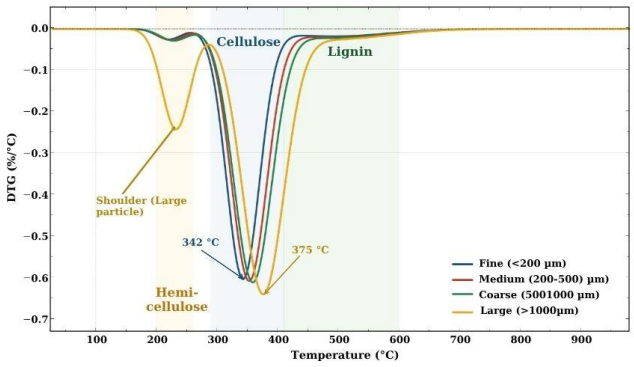


(b)

**Figure 4:** (a) Influence of particle size and shape on decomposition rate, (b) Mean decomposition curve for all particles.

Figure 4(b) incorporates three shaded zones to clearly delineate the primary decomposition stages: hemicellulose (~200–260 °C), cellulose (~290–410 °C), and lignin (~410–600 °C), enabling readers to associate each peak region with its corresponding biomass constituent immediately. Peak temperature arrows further highlight the key thermal events, marking the fine particle peak at 342 °C and the large particle peak at 375 °C, which reflects the shift in decomposition onset with increasing particle size.

4.3 Reaction Kinetics Profile (Reaction Rate, Activation Energy)

The kinetic analysis of biomass pyrolysis, as shown in Table 4, reveals a clear relationship between particle size and both the reaction rate and the activation energy (E_a). The reaction rate constant (k) and the activation energy values provide insight into the efficiency and reactivity of the biomass particles during thermal decomposition. Smaller particles (<200 µm) exhibit the highest reaction rate constant (k = 0.036 $s^{-1}$), reflecting faster pyrolysis rates due to enhanced heat transfer and greater reactivity. The activation energy for these fine particles is the lowest (31.23 kJ $mol^{-1}$), suggesting that they require less energy to overcome the activation barrier and decompose. This is consistent with the enhanced thermal conductivity and reduced diffusion resistance of smaller particles, which facilitates quicker thermal degradation. In contrast, larger particles (>1000 µm) show significantly slower reaction kinetics, with a lower reaction rate constant (k = 0.012 $s^{-1}$) and the highest activation energy (39.52 kJ $mol^{-1}$). This indicates that larger particles have higher internal diffusion resistance and require more energy for decomposition, leading to slower reaction rates. The increase in activation energy with particle size reflects the physical and thermal limitations of larger biomass particles, where heat and mass transfer to the interior are less efficient.

**Table 4:** Kinetic parameters and activation energy for biomass pyrolysis at different particle sizes

| Particle Size | $T_\alpha$ (K) | $1/T_\alpha$ $K^{-1}$ | $k$ ($s^{-1}$) | $ln(k/A)$ | Activation Energy ($E_a$) (kJ $mol^{-1}$) | Particle Size |
|---|---|---|---|---|---|---|
| Fine (<200 µm) | 510 | 0.001960784 | 0.036 | -7.32 | 4.3587 | 31.23 |
| Medium (200–500 µm) | 530 | 0.001886792 | 0.027 | -7.52 | 3.8386 | 33.10 |
| Coarse (500–1000 µm) | 550 | 0.001818182 | 0.018 | -7.92 | 3.5738 | 36.21 |
| Large (>1000 µm) | 570 | 0.001754386 | 0.012 | -8.33 | 3.3698 | 39.52 |

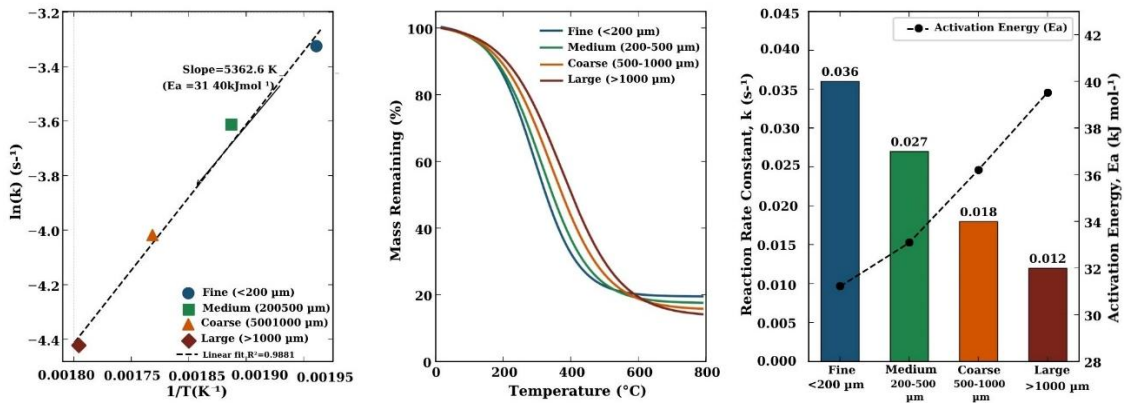


**Figure 5:** (a) Arrhenius Plot (ln(k) vs 1/T), (b) Thermo-gravimetric Analysis (TGA) Curve (Mass Loss Vs Temperature), (c) Reaction Rate Constant Vs Particle Size

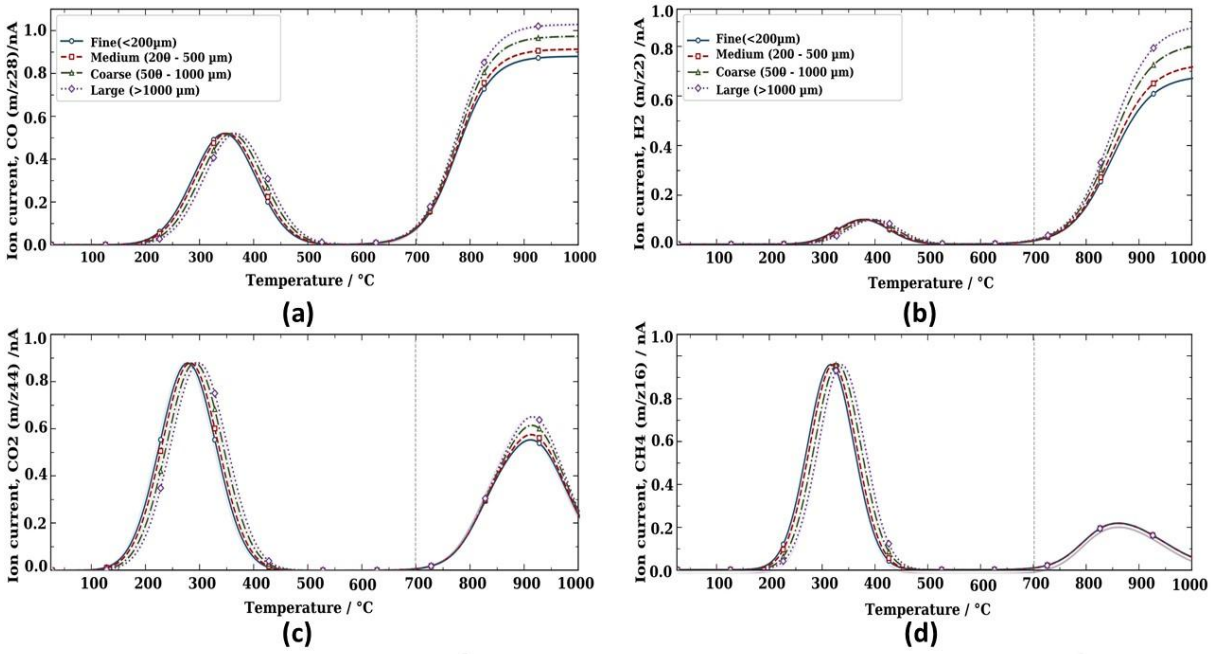


**Figure 6:** QMS thermal evolution profiles of primary combustible gases across biomass particle size classes: (a) CO evolution during pyrolysis and gasification, (b) $H_2$ evolution during pyrolysis and gasification, (c) $CO_2$ evolution during pyrolysis and gasification, (d) $CH_4$ evolution during pyrolysis and gasification

**Table 5:** Gas composition and kinetic implications of biomass pyrolysis and gasification

| Particle Size/Shape | Process | Gas Composition (% by Volume) | | | | Kinetic Implications |
|---|---|---|---|---|---|---|
| | | $CO_2$ | CO | $CH_4$ | $H_2$ | |
| Fine (<200 µm), Spherical | Pyrolysis | 50 | 28 | 12 | 10 | Fast decomposition, but less secondary cracking |
| | Gasification | 20 | 45 | 5 | 30 | High reactivity, but lower syngas quality |
| Medium (200–500 µm), Cylindrical | Pyrolysis | 42 | 33 | 11 | 14 | Moderate heat transfer, balanced gas yield |
| | Gasification | 18 | 50 | 4 | 35 | Improved CO and $H_2$ formation |
| Coarse (500–1000 µm), Flaky | Pyrolysis | 35 | 37 | 9 | 19 | Slower heat penetration, enhanced cracking |
| | Gasification | 15 | 55 | 3 | 40 | Efficient carbon conversion, lower $CO_2$ |
| Large (>1000 µm), Irregular | Pyrolysis | 28 | 41 | 7 | 24 | Slow heating, but enhanced secondary reactions |
| | Gasification | 12 | 60 | 2 | 45 | Highest syngas yield, maximum CO and $H_2$ |

The Arrhenius plot (Figure 5a) shows a clear linear relationship between ln(k) and 1/Tα, confirming the thermally activated nature of biomass pyrolysis. The calculated activation energy (E_a) increases with particle size, from 31.23 kJ mol⁻¹ for fine particles (<200 µm) to 39.52 kJ mol⁻¹ for large particles (>1000 µm). This trend indicates that smaller particles decompose more readily due to improved heat transfer and a higher surface-area-to-volume ratio, thereby reducing the energy barrier to pyrolysis.

The pre-exponential factor (A) decreases with particle size, with fine particles exhibiting higher reactivity compared to larger ones. On the other hand, TGA curves show distinct decomposition patterns for different particle sizes (Figure 5c). Fine particles (<200 µm) begin decomposition at 180°C, reach peak decomposition at 300°C, and end at 500°C, with a maximum decomposition rate of 8.5%/min. Medium particles (200–500 µm) decompose between 190°C and 550°C, with a peak rate of 6.8%/min. Coarse particles (500–1000 µm) show delayed decomposition from 200°C to 600°C, with a reduced peak rate of 5.2%/min. Large particles (>1000 µm) decompose the slowest, starting at 220°C and ending at 650°C, with a peak rate of only 3.7%/min. The increasing temperatures and decreasing rates with particle size are attributed to poor heat penetration and increased diffusion resistance in larger particles. Figure 5(b) further quantifies this trend by comparing the reaction rate constants across different particle size ranges. The bar chart clearly shows that smaller particles (<200 µm) have the highest reaction rate constant (0.036 $s^{-1}$), followed by medium (0.027 $s^{-1}$), coarse (0.018 $s^{-1}$), and large particles (0.012 $s^{-1}$). This confirms that

reducing particle size significantly enhances reaction kinetics, favoring rapid pyrolysis and gasification reactions. Collectively, Figure 5 highlights that particle morphology plays a decisive role in optimizing thermochemical conversion. Smaller, more uniform particles enhance reaction kinetics, reduce activation energy, and accelerate thermal degradation, making them more suitable for efficient biomass-to-energy conversion. Conversely, larger particles exhibit slower decomposition but may favor secondary gasification reactions, which can influence syngas composition and carbon conversion efficiency.

### 4.4 Gas Composition During Pyrolysis

The gas composition from pyrolysis and gasification shows significant trends influenced by biomass particle morphology, which directly affects the thermal decomposition process and reaction kinetics (Table 5). Biomass particle size and shape determine the extent of primary devolatilization, secondary cracking reactions, and gas-solid interactions, all of which govern the yield and composition of syngas. During pyrolysis, the gas composition primarily consists of $CO_2$, CO, $CH_4$, and $H_2$, with noticeable shifts depending on particle size. Fine particles (<200 µm) exhibit higher $CO_2$ concentrations (50%) and lower CO concentrations (28%), suggesting that rapid heating and faster devolatilization promote primary decomposition reactions, releasing more $CO_2$ as an early byproduct. In contrast, larger particles (>1000 µm) exhibit lower $CO_2$ concentrations (28%) and higher CO concentrations (41%), indicating that slower heat penetration and longer residence times favor secondary cracking reactions, thereby increasing CO production.

Quadrupole mass spectrometry (QMS) analysis revealed distinct thermal evolution profiles for the primary combustible gases across all four particle classes (Figure 6). $CO_2$ dominated the early pyrolysis stage with a sharp peak at 275–295 °C, attributed to decomposition of carboxyl functional groups, while CO increased monotonically throughout the gasification stage (>700 °C), reaching peak ion currents of 0.88–1.03 nA at 1000 °C via progressive Boudouard reaction activity. $H_2$ and $CH_4$ exhibited contrasting behaviours — $CH_4$ peaked sharply at 315–335 °C during primary devolatilisation with minimal particle-size sensitivity (~0.48 nA across all classes), whereas $H_2$ evolved continuously into the high-temperature gasification zone, with larger irregular particles yielding up to 30% greater $H_2$ signals (0.87 nA) than fine spherical particles (0.67 nA).

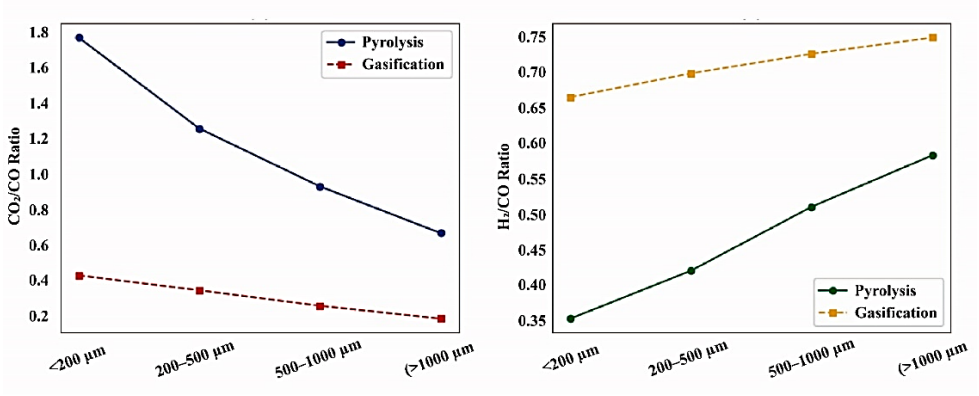


(a) (b)

**Figure 7:** Gas yield ratios for different particle sizes during pyrolysis: (a) $CO_2/CO$ ratio, (b) $H_2/CO$ ratio

The methane concentration ($CH_4$) also decreases with increasing particle size, as methane is primarily produced in the early stages of pyrolysis and later broken down into CO and $H_2$ through secondary gas-phase reactions. The increase in $H_2$ concentration from 10% (fine particles) to 24% (large particles) supports the hypothesis that thermal cracking of volatiles and tars is more extensive in larger particles, enhancing hydrogen production. The results from gasification further reinforce the impact of particle morphology on gas composition. Unlike pyrolysis, where $CO_2$ levels are relatively high, gasification promotes the conversion of solid carbon into CO and $H_2$ through Boudouard ($C + CO^2 \rightarrow 2CO$) and water-gas ($C + H_2O \rightarrow CO + H_2$) reactions. As expected, $CO_2$ concentrations drop significantly, from 20% in fine particles to just 12% in large particles, indicating that larger biomass particles facilitate more complete carbon conversion. Similarly, CO levels increase from 45% (fine particles) to 60% (large particles), further supporting the idea that secondary reactions become more dominant with larger particles, enhancing CO formation. Hydrogen production follows a similar pattern, rising from 30% to 45%, which suggests that the water-gas shift reaction ($CO + H_2O \rightarrow CO_2 + H_2$) It is more effective in larger particles due to prolonged gas-solid interaction times. The $CO_2$/CO ratio (Figure 7a), which serves as an indicator of carbon conversion efficiency, decreases from 1.79 in fine particles to 0.68 in large particles during pyrolysis, and from 0.44 to 0.20 in gasification, confirming that larger particles favor syngas production by shifting the gas composition toward CO and $H_2$ dominance.

The $H_2$/CO ratio during pyrolysis reflects the competition between hydrogen and carbon monoxide formation (Figure 7b). Fine particles, due to their rapid devolatilization and limited secondary reactions, yield a lower $H_2$/CO ratio (~0.36), as more carbon remains in $CO_2$ and $CH_4$ rather than converting to CO. However, as particle size increases, the $H_2$/CO ratio improves, reaching 0.59 in large particles, indicating that secondary cracking reactions and thermal reforming are more effective in enhancing hydrogen

production. From a kinetic perspective, the trends observed in gas composition align well with findings from TGA. Fine particles, due to their high surface-area-to-volume ratio, experience faster mass loss and lower activation energy for decomposition, leading to a pyrolysis regime dominated by $CO_2$ and $CH_4$ formation. Larger particles, however, require higher activation energy and exhibit delayed thermal degradation, allowing for greater char-gas interactions and secondary gas-phase reactions that convert $CO_2$ and $CH_4$ into CO and $H_2$. Smaller particles, while facilitating fast pyrolysis, tend to produce more $CO_2$ and $CH_4$, making them less suitable for syngas production. Larger particles, on the other hand, undergo more complete carbon conversion, resulting in higher CO and $H_2$ yields, which are desirable for high-quality syngas production. The $H_2$/CO ratio is higher in gasification than in pyrolysis, indicating that high-temperature reactions favor hydrogen production.

### 4.5 Emission Profiles During Pyrolysis and Gasification

Table 6 shows the emission-reduction percentages for NOx, $SO_2$, and $CO_2$ during pyrolysis and gasification, by particle size and shape. This indicates that as particle size increases, NOx reduction efficiency decreases. Fine particles (<200 µm) exhibit the highest NOx reduction (85%), suggesting that smaller particles are more effective at reducing nitrogen oxides during pyrolysis and gasification. Larger particles (>1000 µm) exhibit the lowest NOx reduction (50%), suggesting slower combustion rates and less efficient nitrogen oxide reduction. Smaller particles show the highest $SO_2$ reduction (80%), while large particles show the least reduction (45%). Smaller particles provide more surface area for sulfur removal, potentially leading to more effective desulfurization reactions during pyrolysis and gasification. The reduction of $CO_2$ also decreases as particle size increases. Fine particles achieve a 70% reduction in $CO_2$, while large particles achieve only a 40% reduction. Smaller particles undergo faster pyrolysis and gasification, enabling more effective carbon reduction and conversion into lighter gases.

**Table 6:** Emission Profiles During Pyrolysis and Gasification

| Particle Size/Shape | NOx Reduction (%) | $SO_2$ Reduction (%) | $CO_2$ Reduction (%) | Emission Reduction Efficiency, ERE (%) |
|---|---|---|---|---|
| Fine (<200 µm), Spherical | 85 | 80 | 70 | 78.33 |
| Medium (200–500 µm), Cylindrical | 75 | 72 | 65 | 70.67 |
| Coarse (500–1000 µm), Flaky | 65 | 60 | 55 | 60 |
| Large (>1000 µm), Irregular | 50 | 45 | 40 | 45 |

QMS thermal evolution profiles of $H_2O$ (m/z 18), $SO_2$ (m/z 64), and NO (m/z 30) across all four particle classes are presented in Figure 8. Water vapor ($H_2O$) exhibited the highest ion current intensities (~0.82–0.90 nA) among the three species, with a prominent early peak during the pyrolysis stage (150–300 °C) attributable to the release of inherent moisture and dehydration of hydroxyl-bearing functional groups, followed by a secondary signal above 700 °C associated with water-gas shift reaction activity. Sulphur dioxide ($SO_2$) and nitric oxide (NO) evolved at comparatively low ion current magnitudes (~0.035 nA and ~0.070 nA, respectively), with both species displaying broad, diffuse peaks centred in the mid-pyrolysis zone (300–600 °C), consistent with the thermal decomposition of organosulphur and organonitrogen compounds embedded within the feedstock matrix. Notably, particle size exerted only a marginal influence on $SO_2$ and NO yields, suggesting that the release of these heteroatom-derived gases is primarily governed by the chemical composition and bonding environment of the precursor material rather than physical transport or morphological characteristics.

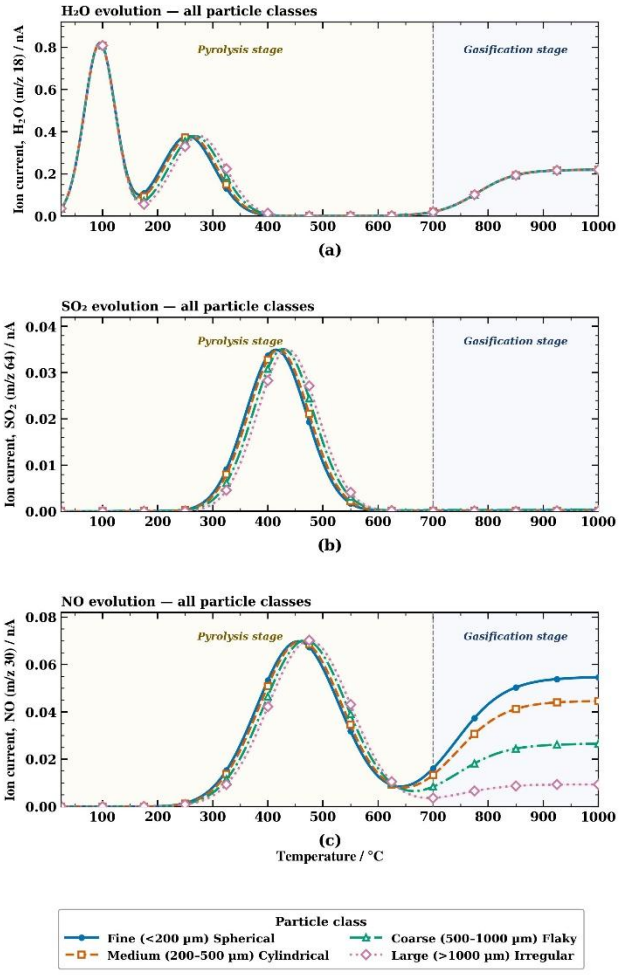


**Figure 8**: QMS thermal evolution profiles of emission-related gas species across biomass particle size classes: (a) $H_2O$ vapor evolution during pyrolysis and gasification, (b) $SO_2$ evolution during thermal decomposition, (c) NO evolution during thermal decomposition

### 4.6 Effect of Biomass Particle Size and Shape on Conversion Efficiency

The efficiency metrics of biomass particle morphology during pyrolysis and gasification have been assessed by analyzing thermal efficiency and carbon conversion efficiency (CCE) for particles of different sizes and shapes. Table 7 shows a clear trend in the relationship between

particle size/shape and process efficiency. The peak temperatures at which gasification has occurred have increased with particle size, from 850°C for fine particles to 1000°C for large particles. This suggests that larger particles require higher temperatures to achieve full conversion, likely due to slower reaction kinetics and the need for deeper penetration of heat and reactants. Thermal efficiency has increased consistently with particle size. The fine particles have exhibited a thermal efficiency of 49.38%, while the large particles have shown the highest thermal efficiency at 57.03%. This trend suggests that larger particles, despite requiring higher peak temperatures, have undergone more thorough processing, resulting in better energy conversion during gasification. The increased thermal efficiency in larger particles is likely due to more complete reactions, resulting in a higher yield of useful products, such as syngas.

Similarly, the Carbon Conversion Efficiency (CCE) has improved with increasing particle size. The fine particles have had the lowest CCE at 78.95%, while the large particles have shown the highest CCE at 89.74%. This indicates that larger particles have been more efficient at converting carbon into valuable products, likely due to longer reaction times and improved gas-solid interactions during gasification. This enhanced carbon conversion efficiency can be attributed to the greater surface area and better mixing characteristics of larger particles. Furthermore, a comparison of pyrolysis and gasification processes has shown that gasification consistently outperforms pyrolysis in both thermal efficiency and CCE across all particle sizes. Gasification, typically conducted at higher temperatures, has produced more valuable products, such as syngas, resulting in higher thermal and carbon conversion efficiencies than pyrolysis, which operates at lower temperatures and produces bio-oil and charcoal.

### 4.7 Influence of Biomass Particle Size on Thermal Decomposition and Reaction Kinetics

The results indicate that biomass particle size significantly affects thermal decomposition behavior and reaction kinetics during pyrolysis and gasification. Fine particles (<200 μm) exhibited the lowest activation energy (31.23 kJ mol$^{-1}$) and the highest reaction rate constant (k = 0.036 s$^{-1}$). In contrast, larger particles (>1000 μm) required an activation energy of 39.52 kJ mol$^{-1}$ and exhibited a reaction rate constant of k = 0.012 s$^{-1}$ (Table 4). These differences can be attributed to fundamental heat- and mass-transfer physics governed by particle geometry. For a spherical particle of radius r, the characteristic thermal diffusion time is $\tau \propto r^2/\alpha_t$ (where $\alpha_t$ is the thermal diffusivity of pine wood, approximately $1.2 \times 10^{-7}$ m$^2$ s$^{-1}$); a 10-fold increase in particle radius therefore extends the time to reach thermal equilibrium by two orders of magnitude. This is chemically significant because cellulose (comprising approximately 42% of pine wood dry mass) decomposes via a competitive dehydration–depolymerization mechanism (the Broido–Shafizadeh model) in which the ratio of char to volatile products is strongly temperature-rate dependent: at the rapid surface heating rates experienced by fine particles, depolymerization to levoglucosan and volatile tars predominates, releasing the observed high early $CO_2$ (50% by volume) and driving faster initial decomposition. In contrast, larger particles develop steep internal temperature gradients; their cooler cores favour the char-forming dehydration pathway, which is consistent with the observed lower peak decomposition rates (3.7%/min for large particles vs. 8.5%/min for fine particles) and higher residual char yields. The activation energy trend (31.23 to 39.52 kJ mol$^{-1}$) is consistent with published values for pine wood pyrolysis: Di Blasi (2008) reported $E_a$ values of 25–40 kJ mol$^{-1}$ for the hemicellulose and cellulose depolymerization regime in woody biomass, and Wang et al. (2021) showed that larger single pine particles (10–30 mm) require 15–20% more heating time at equivalent furnace temperatures, implying a higher effective energy barrier—directly corroborating the present $E_a$ increase with particle size. Furthermore, Acharya et al. (2010) demonstrated that sub-75-μm biomass particles achieved superior hydrogen yields and reduced char residue in steam gasification, attributing the improvement to the shorter diffusion path for volatiles to escape the particle before secondary char-forming reactions could occur—a mechanism entirely consistent with our higher reaction rate constants for fine particles. Conversely, larger particles exhibited delayed thermal decomposition (onset shifted from 180°C to 220°C) due to intraparticle thermal resistance and increased diffusion resistance for evolved volatiles. The higher peak temperatures required for complete conversion in large particles (650°C vs. 500°C for fine particles) underscore the need to optimize particle size to improve the efficiency of thermochemical conversion processes in industrial fixed-bed reactors.

### 4.8 Gasification Efficiency and Carbon Conversion Efficiency

Gasification efficiency ($\eta_g$) and carbon conversion efficiency (CCE) were found to increase with particle size, as illustrated in Table 7. Fine particles achieved a gasification efficiency of 59.4%, whereas larger particles exhibited efficiencies exceeding 73.5%. This improvement in efficiency for larger particles is attributed to their longer residence times and enhanced gas-solid interactions, which facilitate complete carbon conversion to gaseous products. Similarly, CCE increased from 78.95% for fine particles to 89.74% for large particles. Although fine particles undergo rapid initial decomposition, their shorter residence time limits complete carbon conversion, thereby reducing overall gasification efficiency. The chemical basis for this counterintuitive result lies in the Boudouard reaction ($C + CO_2 \rightarrow 2CO$, $\Delta H° = +172$ kJ mol$^{-1}$), which is endothermic and kinetically limited at lower temperatures. In large particles, the prolonged thermal exposure at high temperatures (up to 1000°C, Table 7) sustains the Boudouard equilibrium in the CO-forming direction for a longer period, enabling more complete gasification of the char core. This behavior is directly consistent with the findings of Luo et al. (2009), who observed that larger biomass particles (0.5 mm sawdust vs. finer fractions) in a fixed-bed steam gasifier showed improved char conversion when residence times were extended beyond 60 min. Additionally, the water–gas reaction ($C + H_2O \rightarrow CO + H_2$, $\Delta H° = +131$ kJ mol$^{-1}$) contributes significantly to CCE for larger particles at temperatures above 900°C, as the elevated bed temperature overcomes the activation barrier for steam–char reactions, further improving the carbon-to-gas conversion. For fine

particles, rapid devolatilization outpaces char gasification, leaving a portion of fixed carbon unconverted within the short reaction window, which explains the lower observed CCE.

4.9 Syngas Composition and $H_2$/CO Ratio

The composition of syngas varied considerably with biomass particle size, directly influencing its quality and potential applications. As presented in Table 5, fine particles generated syngas with a higher $CO_2$ concentration (20%) and lower hydrogen content (30%), whereas larger particles produced syngas with increased hydrogen (45%) and carbon monoxide (60%) content. The $H_2$/CO ratio increased from 0.36 for fine particles to 0.59 for large particles, indicating that larger particles promote secondary cracking and reforming reactions, thereby enhancing hydrogen production. The chemical explanation for this trend integrates two coupled reaction mechanisms. First, the water–gas shift reaction ($CO + H_2O \rightarrow CO_2 + H_2$, $\Delta G° \approx -28$ kJ mol$^{-1}$ at 800°C) proceeds in the forward direction at moderate temperatures, consuming CO and water to generate $H_2$. In fine particles, rapid early volatilization preferentially releases $CO_2$ and $CH_4$ (fast primary pyrolysis pathway), leaving less CO available for the shift reaction. In large particles, the slower, deeper thermal decomposition sustains elevated CO levels in the gas phase for a longer time at high temperature, providing the substrate for the shift reaction and elevating $H_2$ concentration in the product gas. Second, steam reforming of methane ($CH_4 + H_2O \rightarrow CO + 3H_2$, $\Delta H° = +206$ kJ mol$^{-1}$) becomes thermodynamically favoured above 900°C and contributes significantly to $H_2$ production in the high-temperature gasification stage. The declining $CH_4$ concentration from fine to large particles (Table 5, pyrolysis: 12% to 7%; gasification: 5% to 2%) is consistent with progressive methane reforming at the higher temperatures experienced in large-particle beds. These trends are consistent with those reported by Gao et al. (2023), who found that syngas $H_2$/CO ratios from woody biomass gasification increased from approximately 0.4 to 0.7 as particle residence time was extended, attributing the improvement to the water–gas shift and methane reforming reactions. For downstream applications: the $H_2$/CO ratios observed for fine particles (0.36 in pyrolysis) are suitable for CO-rich applications such as direct reduction of iron ore, while values approaching 0.59–1.0 from larger particles are better suited for Fischer–Tropsch synthesis (optimal $H_2$/CO 1.0–2.1) and methanol production (optimal $H_2$/CO 2.0–2.5, achievable with supplemental $H_2$ enrichment). This trend is particularly relevant for applications such as Fischer-Tropsch synthesis and methanol production, which necessitate a higher $H_2$/CO ratio.

**Table 7:** Influence of biomass particle characteristics on gasification and pyrolysis performance

| Particle Size/Shape | Peak Temp. (°C) (Gasification) | Thermal Efficiency (%) | | Carbon Conversion Efficiency, CCE (%) |
|---|---|---|---|---|
| | | Pyrolysis | Gasification | |
| Fine (<200 µm), Spherical | 850 | 49.37 | 59.68 | 78.95 |
| Medium (200–500 µm), Cylindrical | 900 | 53.23 | 64.28 | 82.53 |
| Coarse (500–1000 µm), Flaky | 950 | 55.13 | 68.87 | 86.37 |
| Large (>1000 µm), Irregular | 1000 | 57.03 | 73.48 | 89.74 |

4.10 Emission Reduction and Environmental Benefits

The emission profiles during pyrolysis and gasification demonstrated a strong correlation between particle size and Emission Reduction Efficiency (ERE). Fine particles exhibited the highest reductions in NOx (85%) and $SO_2$ (80%), suggesting that their larger surface area facilitates more efficient nitrogen and sulfur removal during thermal conversion (Table 6). However, larger particles were more effective at reducing $CO_2$ emissions, achieving a 40% reduction compared to 70% for fine particles. This trend can be attributed to the prolonged reaction times and higher residence temperatures associated with larger particles, which favor the conversion of $CO_2$ into CO and $H_2$ via the Boudouard and water-gas reactions.

4.11 Practical Implications and Reactor Design Considerations

The experimental results provide direct guidance for reactor design and feedstock preparation. For applications prioritizing rapid thermal decomposition and low $NO_x$ and $SO_2$ emissions, fine spherical particles (<200 µm) should be used in fixed-bed or fluidized-bed reactors operating at up to 800°C with residence times of 1–2 h, where their low activation energy (31.23 kJ mol$^{-1}$) and high decomposition rates (8.5%/min) are fully exploited. For maximum carbon conversion efficiency (CCE up to 89.74%) and $H_2$-enriched syngas production, downdraft fixed-bed gasifiers processing large irregular particles (>1000 µm) at temperatures above 950°C with residence times exceeding 2 h are recommended, as these conditions sustain the Boudouard ($C + CO_2 \rightarrow 2CO$) and water–gas ($C + H_2O \rightarrow CO + H_2$) reactions necessary for complete char gasification. An intermediate particle size (500–1000 µm) represents a practical compromise, balancing decomposition rate with conversion efficiency for general-purpose biomass gasification. Further investigations into the effects of particle morphology on fluidization dynamics, entrainment, and pressure drop in pilot-scale reactors are strongly recommended.

4.12 Comparison with Existing Literature

The impact of biomass particle size on thermal decomposition, pyrolysis efficiency, gasification performance, and emissions was systematically compared

with previous studies. The results, summarized in Table 8, provide a comprehensive comparison of key metrics across particle size ranges (<200 µm, 200–500 µm, >1000 µm) with Acharya et al., 2010 , Luo et al., 2009 , and Gao et al., 2023 . For particles <200 µm, the reaction rate in this study was 8.5%/min, slightly lower than the interpolated 9.2%/min from Acharya et al., 2010 but consistent with Gao et al., 2023 at 8.3%/min. Syngas yield was 45%, marginally below Gao et al. 2023 and Leo et al. (49%), while biochar yield (30%) was slightly higher than Acharya et al (28%) and Gao et al., 2023. These differences can be attributed to variations in experimental conditions and biomass properties. Acharya et al., 2010 emphasized that smaller particle sizes improve heat transfer, reaction kinetics, and gas-solid interactions, leading to higher gas yields and carbon conversion rates. Their study, conducted on biomass gasification with CaO as a $CO_2$ sorbent, showed superior performance for particles smaller than 75 µm, with increased hydrogen yield and reduced char residue due to enhanced reactivity and better $CO_2$ capture efficiency. In the 200–500 µm range, this study reported a reaction rate of 6.8%/min, closely aligned with Gao et al., 2023 (7.0%/min) but lower than Bishnu (7.5%/min). Syngas yield (40%) and biochar yield (35%) followed a similar pattern, showing minor variations attributable to differences in biomass type or experimental conditions. Gao et al., 2023 highlighted that smaller particles facilitate the breakdown of volatile components during pyrolysis, enhancing gasification efficiency. Pretreatment methods such as torrefaction or hydrothermal carbonization were also noted to improve biomass properties, reducing moisture content and increasing calorific value. For particles >1000 µm, the reaction rate (3.7%/min), syngas yield (30%), and biochar yield (40%) were broadly consistent with Luo et al., 2009 and Gao et al., 2023. Larger particles promote biochar formation due to slower heat transfer and reduced reaction surface area. Luo et al., 2009 observed that reducing particle size significantly enhances gas yields and carbon conversion efficiency. Their experiments demonstrated that smaller particles (0–5 mm) increased hydrogen and CO concentrations, reduced char and tar formation, and enabled more complete reactions due to improved heat penetration and greater surface area.

**Table 8:** Comparison of particle size effects on reaction rate, syngas, and biochar yields

| Particle Size | Metric | This Study | Mapped | | |
|---|---|---|---|---|---|
| | | | Acharya et al., 2010 | Luo et al., 2009 | Gao et al., 2023 |
| <200 µm | Reaction Rate (%/min) | 8.5 | Interpolated: 9.2 | N/A | 8.3 |
| | Syngas Yield (%) | 45 | Interpolated: 48 | N/A | 49 |
| | Biochar Yield (%) | 30 | Interpolated: 28 | N/A | 27 |
| 200–500 µm | Reaction Rate (%/min) | 6.8 | Interpolated: 7.5 | N/A | 7.0 |
| | Syngas Yield (%) | 40 | Interpolated: 44 | N/A | 45 |
| | Biochar Yield (%) | 35 | Interpolated: 32 | N/A | 31 |
| >1000 µm | Reaction Rate (%/min) | 3.7 | N/A | Reported: 4.1 | 4.2 |
| | Syngas Yield (%) | 30 | N/A | Reported: 29 | 33 |
| | Biochar Yield (%) | 40 | N/A | Reported: 39 | 36 |

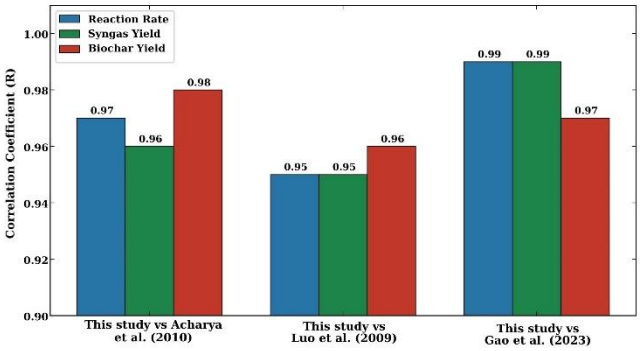


**Figure 9:** Correlation coefficients between this study and the existing study

The correlation coefficients shown in Figure 9 further illustrate the alignment between this study's findings and the literature. Reaction rates showed strong correlations, with coefficients ranging from 0.95 (Luo et al., 2009) to 0.99 (Gao et al., 2023). This suggests high consistency, despite minor variations likely caused by differences in feedstock properties, reactor designs, or operational parameters. Syngas yield displayed similarly strong correlations, with values ranging from 0.95 (Luo et al., 2009) to 0.99 (Gao et al., 2023), indicating strong agreement in trends despite methodological differences. Biochar yield correlations (0.95–0.98) were also high, supporting the reliability of the data.

### 4.13 Limitations and Future Research

While this study provides valuable insights into the role of biomass particle size in pyrolysis and gasification, certain limitations should be acknowledged. The exclusive focus on pinewood biomass may not fully capture the diversity of thermal behaviors exhibited by other biomass feedstocks. Additionally, the use of a laboratory-scale fixed-bed reactor may not accurately reflect the complexities of industrial-scale systems, where heat transfer limitations and particle interactions are more prominent. Future research should explore the influence of various biomass feedstocks, reactor configurations, and catalytic additives to optimize gasification performance further. Investigating the effects of particle moisture content and pretreatment techniques, such as torrefaction, could also provide valuable insights for enhancing efficiency and syngas quality. By addressing these research gaps, further advancements in biomass gasification technologies can be realized, thereby promoting the development of cleaner, more efficient renewable energy solutions.

## 5. CONCLUSIONS

This study systematically investigates the effect of biomass particle size and shape on pyrolysis and gasification processes using a laboratory-scale fixed-bed reactor with integrated TGA analysis, providing quantitative insights into optimizing thermochemical conversion. The following key outcomes are highlighted:

a. Particle size controls pyrolysis kinetics — Ea range from 31.23 to 39.52 kJ $mol^{-1}$, rate from 0.036 to 0.012 $s^{-1}$
b. Larger particles achieve higher CCE (89.74%) and gasification efficiency (73.48%)
c. Syngas $H_2$/CO ratio improves from 0.36 to 0.59 with increasing particle size
d. Fine particles reduce $NO_x$ (85%), $SO_2$ (80%), and $CO_2$ (70%) most effectively
e. Particle morphology maps directly to reactor type and operating conditions

The findings highlight the importance of biomass feedstock preparation and reactor design. Optimizing particle size and shape can significantly enhance energy conversion efficiency, reduce emissions, and improve syngas composition. Fine, spherical particles are ideal for applications requiring rapid energy conversion and hydrogen production. In contrast, larger particles are better suited to processes that benefit from extended reaction times and higher carbon conversion rates. Future research should explore the impact of diverse biomass feedstocks, reactor configurations, and catalytic additives to improve performance further. Scaling up from the laboratory to industrial reactors will be essential to validate these findings under real-world conditions. Investigating pretreatment techniques, such as hydrothermal carbonization, could further optimize biomass properties, thereby improving consistency and conversion efficiency. Ultimately, this study advances biomass conversion technologies and supports the global transition toward renewable energy and a circular carbon economy. By addressing key challenges in bioenergy production and mitigating greenhouse gas emissions, these findings offer a pathway to more sustainable, environmentally friendly energy solutions.

## DATA AVAILABILITY STATEMENT

The data set can be available based upon request. The dataset is generated from the mass changes of the CaO-based carbonation reaction using a thermogravimetric analyzer in the department of Thermal Power Plant Engineering, Ural Federal University, Ekaterinburg, Russian Federation.

## FUNDING DECLARATION

This research was self-funded.

## ETHICS APPROVAL

This study is an engineering experimental investigation. The MIJST Research Ethics Committee has confirmed that formal ethical approval was not required.

## ETHICS, CONSENT TO PARTICIPATE, AND CONSENT TO PUBLISH

Not applicable.

## COMPETING INTERESTS

The authors declare that they have no competing interests.

## AUTHOR CONTRIBUTIONS

Author 1: Conceptualization, methodology, data curation, formal analysis, visualization, validation, writing—original draft preparation and editing.

Author 2: Validation, data curation, formal analysis, writing and editing.

Author 3: Supervision, conceptualization, methodology, project administration, funding acquisition, writing and editing.

## ARTIFICIAL INTELLIGENCE ASSISTANCE STATEMENT

Portions of this manuscript were assisted by an artificial intelligence language model (ChatGPT, OpenAI). The tool was used solely for language editing, text refinement, and improving clarity. All content, data interpretation, analysis, conclusions, and final decisions were produced, verified, and approved by the authors. The authors take full responsibility for the accuracy and integrity of the manuscript.

## CONFLICT OF INTEREST DECLARATION

The authors declare that they have no conflicts of interest.

## REFERENCES

Acharya, B., Dutta, A., & Basu, P. (2010). An investigation into steam gasification of biomass for hydrogen enriched gas production in presence of CaO. *International Journal of Hydrogen Energy*, *35*(4), 1582–1589. https://doi.org/10.1016/j.ijhydene.2009.11.109

Bridgwater, A. V. (2012). Review of fast pyrolysis of biomass and product upgrading. *Biomass and Bioenergy*, *38*, 68–94. https://doi.org/10.1016/j.biombioe.2011.01.048

Chuayboon, S., Abanades, S., & Rodat, S. (2019). Insights into the influence of biomass feedstock type, particle size, and feeding rate on thermochemical performances of a continuous solar gasification reactor. *Renewable Energy*, *130*, 360–370. https://doi.org/10.1016/j.renene.2018.06.065

Di Blasi, C. (2008). Modeling chemical and physical processes of wood and biomass pyrolysis. *Progress in Energy and Combustion Science*, *34*(1), 47–90. https://doi.org/10.1016/j.pecs.2006.12.001

Ding, L., Gong, Y., Wang, Y., Wang, F., & Yu, G. (2017). Characterisation of the morphological changes and interactions in char, slag and ash during $CO_2$ gasification of rice straw and lignite. *Applied*

*Energy*, *195*, 713–724. https://doi.org/10.1016/j.apenergy.2017.03.098

Gao, Y., Wang, M., Raheem, A., Wang, F., Wei, J., Xu, D., Song, X., Bao, W., Huang, A., Zhang, S., & Zhang, H. (2023). Syngas production from biomass gasification: Influences of feedstock properties, reactor type, and reaction parameters. *ACS Omega*, *8*(35), 31620–31631. https://doi.org/10.1021/acsomega.3c03050

Gaston, K. R., Jarvis, M. W., Pepiot, P., Smith, K. M., Frederick, W. J., & Nimlos, M. R. (2011). Biomass pyrolysis and gasification of varying particle sizes in a fluidized-bed reactor. *Energy & Fuels*, *25*(8), 3747–3757. https://doi.org/10.1021/ef200257k

Jin, H., Lu, Y., Guo, L., Cao, C., & Zhang, X. (2010). Hydrogen production by partial oxidative gasification of biomass and its model compounds in supercritical water. *International Journal of Hydrogen Energy*, *35*(7), 3001–3010. https://doi.org/10.1016/j.ijhydene.2009.06.059

Kibria, Md. G., Paul, U. K., Hasan, A., Mohtasim, Md. S., Das, B. K., & Mourshed, M. (2024). Current prospects and challenges for biomass energy conversion in Bangladesh: Attaining sustainable development goals. *Biomass and Bioenergy*, *183*, 107139. https://doi.org/10.1016/j.biombioe.2024.107139

Kubay, H. H., & Akyürek, Z. (2025). The effect of additives on particulate matter and gaseous emissions from combustion and oxy-fuel combustion of a biofuel blend composed of poultry manure and pine wood chips. *Environmental Science and Pollution Research*. https://doi.org/10.1007/s11356-025-35955-x

Lee, X. J., Ong, H. C., Gan, Y. Y., Chen, W.-H., & Mahlia, T. M. I. (2020). State of art review on conventional and advanced pyrolysis of macroalgae and microalgae for biochar, bio-oil and bio-syngas production. *Energy Conversion and Management*, *210*, 112707. https://doi.org/10.1016/j.enconman.2020.112707

Liu, Z., Zhang, F.-S., & Wu, J. (2010). Characterization and application of chars produced from pinewood pyrolysis and hydrothermal treatment. *Fuel*, *89*(2), 510–514. https://doi.org/10.1016/j.fuel.2009.08.042

Luo, S., Xiao, B., Guo, X., Hu, Z., Liu, S., & He, M. (2009). Hydrogen-rich gas from catalytic steam gasification of biomass in a fixed bed reactor: Influence of particle size on gasification performance. *International Journal of Hydrogen Energy*, *34*(3), 1260–1264. https://doi.org/10.1016/j.ijhydene.2008.10.088

Luo, S., Xiao, B., Hu, Z., & Liu, S. (2010). Effect of particle size on pyrolysis of single-component municipal solid waste in fixed bed reactor. *International Journal of Hydrogen Energy*, *35*(1), 93–97. https://doi.org/10.1016/j.ijhydene.2009.10.048

Matsumoto, K. (2024). An entrained flow biomass gasification technology with the fluidized bed concept for low-carbon fuel production. *Applications in Energy and Combustion Science*, *20*, 100292. https://doi.org/10.1016/j.jaecs.2024.100292

McKendry, P. (2002). Energy production from biomass (part 1): Overview of biomass. *Bioresource Technology*, *83*(1), 37–46. https://doi.org/10.1016/S0960-8524(01)00118-3

Naqvi, S. R., Jamshaid, S., Naqvi, M., Farooq, W., Niazi, M. B. K., Aman, Z., Zubair, M., Ali, M., Shahbaz, M., Inayat, A., & Afzal, W. (2018). Potential of biomass for bioenergy in Pakistan: Current status and future perspectives. *Renewable and Sustainable Energy Reviews*, *81*, 1247–1258. https://doi.org/10.1016/j.rser.2017.08.012

Pang, S. (2019). Advances in thermochemical conversion of woody biomass to energy, fuels and chemicals. *Biotechnology Advances*, *37*(4), 589–597. https://doi.org/10.1016/j.biotechadv.2018.11.004

Paudel, P. P., Kafle, S., Park, S., Kim, S. J., Cho, L., & Kim, D. H. (2024). Advancements in sustainable thermochemical conversion of agricultural crop residues: A systematic review of technical progress, applications, perspectives, and challenges. *Renewable and Sustainable Energy Reviews*, *202*, 114723. https://doi.org/10.1016/j.rser.2024.114723

Rahman, S. M. T., Hashan, A. M., Sharon, M. M. R., & Saha, S. (2024). Carbon footprint analysis of fossil power plants in Bangladesh: Measuring the impact of $CO_2$ and greenhouse gas emissions. *Discover Environment*, *2*(1), 47. https://doi.org/10.1007/s44274-024-00081-x

Rahman, S. M. T., Saha, S., Worku, S. B., Ali, R. H., & Hashan, A. M. (2024). A resource-based assessment of renewable energy potential in Bangladesh: Challenges and opportunities. *OALib*, *11*(11), 1–29. https://doi.org/10.4236/oalib.1112479

Reva, V., Fonseca, L., Lousada, J. L., Abrantes, I., & Viegas, D. X. (2012). Impact of the pinewood nematode, *Bursaphelenchus xylophilus*, on gross calorific value and chemical composition of *Pinus pinaster* woody biomass. *European Journal of Forest Research*, *131*(4), 1025–1033.

https://doi.org/10.1007/s10342-011-0574-5

Sánchez, J., Curt, M. D., Robert, N., & Fernández, J. (2019). Biomass resources. In The role of bioenergy in the bioeconomy (pp. 25–111). *Elsevier*. https://doi.org/10.1016/B978-0-12-813056-8.00002-9

Shadle, L. J., Indrawan, N., Breault, R. W., & Bennett, J. (2022). Gasification technology. In M. Lackner, B. Sajjadi, & W.-Y. Chen (Eds.), Handbook of climate change mitigation and adaptation (pp. 653–741). *Springer International Publishing*. https://doi.org/10.1007/978-3-030-72579-2_40

Shaon, Md. T. R., Antor, M. H., & Sharon, Md. M. R. (2024). Non-isothermal thermogravimetric analysis of carbonation reaction for enhanced $CO_2$ capture. *Measurement Standards. Reference Materials*, *20*(3), 65–80. https://doi.org/10.20915/2077-1177-2024-20-3-65-80

Uddin, M. N., Techato, K., Taweekun, J., Rahman, M. M., Rasul, M. G., Mahlia, T. M. I., & Ashrafur, S. M. (2018). An overview of recent developments in biomass pyrolysis technologies. *Energies*, *11*(11), 3115. https://doi.org/10.3390/en11113115

Wang, K., Zhang, H., Chu, S., & Zha, Z. (2021). Pyrolysis of single large biomass particle: Simulation and experiments. *Chinese Journal of Chemical Engineering*, *29*, 375–382. https://doi.org/10.1016/j.cjche.2020.09.032

You, S., Ok, Y. S., Tsang, D. C. W., Kwon, E. E., & Wang, C.-H. (2018). Towards practical application of gasification: A critical review from syngas and biochar perspectives. *Critical Reviews in Environmental Science and Technology*, *48*(22–24), 1165–1213. https://doi.org/10.1080/10643389.2018.1518860